Nanotechnology

Highly Ordered SnO_2 Nanorod Arrays from Controlled Aqueous Growth**

Lionel Vayssieres and Michael Graetzel*

Besides the conventional nanorods, nanowires, and nanotubes,[1] a plethora of new 1D nanomaterials, that is, nanobelts, nanoribbons, nanodisks, nanosheets, and nanodendrites have emerged recently.[1a] Such accomplishments confirm the tremendous efforts spread worldwide to create advanced and functional building blocks for the development of innovative nanomaterials and smart nanodevices. However, the hierarchical design of well-defined and highly oriented 3D arrays of conventional 1D nanomaterials such as nanorods and nanowires in general, and their large-scale manufacturing at low cost in particular, remain crucial challenges to unfold the very promising future of nanotechnology. In addition to the economical manufacturing of nanomaterials, a better fundamental knowledge of their electronic structure, physical, interfacial, and structural properties, as well as their stability is required to fully exploit their fascinating physical and chemical potential. To fulfill such essential requirements, the creation of stable and structurally well-defined and well-ordered nanomaterials at low cost is essential.

Tin(IV) dioxide, SnO_2 (also called stannic oxide) is an insulator and an important, colorless, low-cost, large-bandgap (n-type) semiconductor material when doped with oxygen vacancies or with Sb or F ions. It is widely used as a transparent conducting oxide (TCO) substrate [2] and gas sensor[3] as well as electrode material for energy conversion[4] and storage applications.[4a] Thus, the design of SnO_2 1D nanomaterials with novel and well-defined morphologies and, in particular, as highly ordered 3D arrays, is of noteworthy importance for basic fundamental research as well as of relevance for various fields of industrial and high-tech applications.

[*] Dr. L. Vayssieres
Photonics and Interface Laboratory
Institute of Chemical Sciences and Engineering
Swiss Federal Institute of Technology (EPFL)
1015 Lausanne (Switzerland)
and
International Center for Young Scientists
National Institute for Materials Science
Namiki 1-1, Tsukuba, Ibaraki 305-0044 (Japan)
Fax: (+81) 298-604-706
E-mail: vayssieres.lionel@nims.go.jp
Prof. M. Graetzel
Photonics and Interface Laboratory
Institute of Chemical Sciences and Engineering
Swiss Federal Institute of Technology (EPFL)
1015 Lausanne (Switzerland)

[**] This work was supported by the Swiss National Science Foundation under the NRP 47 program. K. Schenk (Laboratoire de Cristallographie) as well as I. Brauer and P. Stadelman (Centre Interdisciplinaire de Microscopie Electronique) from the Ecole Polytechnique Fédérale de Lausanne are acknowledged for their assistance.

  DOI: 10.1002/ange.200454000

Hitherto, several reports have described the fabrication of powders of SnO_2 nanorods by various techniques that involve a microemulsions,[5] redox reactions,[6] thermal decomposition of oxalate in air[7] or in solution,[8] vapor–liquid–solid (VLS) catalytic growth,[9] laser ablation,[10] thermal evaporation[11] or oxidation of metallic tin.[12] However, only one method has been reported for the creation of SnO_2 oriented nanorod arrays.[13] This synthesis involves conventional processing by using template techniques, that is, electrodeposition and thermal oxidation in an anodic alumina membrane. However, the morphology of the nanorods is rather ill-defined as a result of the processing technique. We report herein a simple, one-step, aqueous, low-temperature growth process for the inexpensive fabrication of large (several tens of cm^2) 3D arrays of highly ordered and crystalline SnO_2 nanorods of typically 50 nm in width and 500 nm in length with a uniquely designed architecture and without the need of template, surfactant, applied field, or undercoating on various substrates. Well-defined and perpendicularly oriented crystalline nanorods with a square cross section (elongated along the *c* axis and exhibiting (110) prismatic faces) are obtained directly on polycrystalline, single-crystalline, or amorphous substrates from the controlled heteronucleation of SnO_2 by aqueous precipitation of Tin(IV) salts at mild temperatures (i.e., below 100 °C) in the presence of urea.

The thermodynamically stable crystal structure of SnO_2 is rutile (tetragonal crystal system), which occurs in nature as the native mineral cassiterite, the principal ore of tin. Cassiterite is isostructural to rutile (TiO_2), argutite (GeO_2), paratellurite (TeO_2), plattnerite (PbO_2), stishovite (SiO_2) and pyrolusite (MnO_2) as well as VO_2, CrO_2, RuO_2, NbO_2, TaO_2, OsO_2, and IrO_2. SnO_2 crystallizes in point group symmetry $4/mmm$ and space group $P4_2/mnm$ (D_{4h}^{14}) with tin and oxygen atoms in 2a and 4f positions, respectively. The unit cell consists of two tin atoms and four oxygen atoms. Each metal atom is situated amidst six oxygen atoms, which approximately form the corners of a regular octahedron. Oxygen atoms are surrounded by three tin atoms, which approximate the corners of an equilateral triangle. Two of each twelve octahedral edges are shared with other octahedra. Edge sharing is symmetrical; the shared edges are opposite each other in the rutile structure. Thus, the octahedra form linear chains, and these chains run parallel to the *c* axis and combine by sharing two opposed edges per octahedron. Each of these chains is surrounded and cross-linked to four identical octahedral chains that twisted at 90° to the first chain. Adjacent chains are all staggered *c*/2 by the 4_2 screw axes that are oriented along tunnels that are parallel to the *c* axis. Consequently, the highest electron density as well as high polarizability and birefringence is observed along the *c* axis. Typical lattice parameters are $a = 4.737$ Å, and $c = 3.186$ Å yielding an axial ratio of $a{:}c = 1{:}0.672$. The low index (110) face is the thermodynamically most-stable bulk termination[14] and has the lowest surface energy,[14a] that is, the surface excess free energy per unit area. The sequence of surface energy per crystal face is $(110) < (100) < (101) \ll (001)$. The (110) stoichiometric surface, in which a half of the surface cations are fivefold coordinated with oxygen atoms and the other half are sixfold coordinated because of the presence of a row of bridging oxygen atoms, yields tin atoms with a formal oxidation state of +IV. Thus, surface and bulk have similar resistivity. The (110) surface has no net dipole moment in the [110] direction and is therefore a nonpolar surface. Additionally, this centrosymmetric structure of low axial ratios reduces substantially the probability of anisotropic growth of the crystal along the [001] direction, and thus reduces the generation of *c*-elongated prismatic crystals. For this reason, SnO_2 1D nanostructures seldom grow along the *c* axis but rather along the [101],[1,7,15] [301],[9,15a] [200],[10] or [11−2][5] directions. However, by allowing a slow generation of nuclei by chemical means as well as a slow nucleation and growth at low interfacial tension conditions (thermodynamic stability), stable *c*-elongated anisotropic nanocrystals exhibiting stable (110) faces may be generated. Thus, according to crystal-symmetry and surface-energy considerations, a typical crystal habit should be acicular and tabular and should exhibit a square cross section (Figure 1). In addition, if such a mechanism were operative directly at the surface of a substrate (single or polycrystalline, or amorphous), which represents a reduced surface-energy barrier compared to homogeneous nucleation, highly oriented nanorods would grow with normal incidence onto the substrate surface.

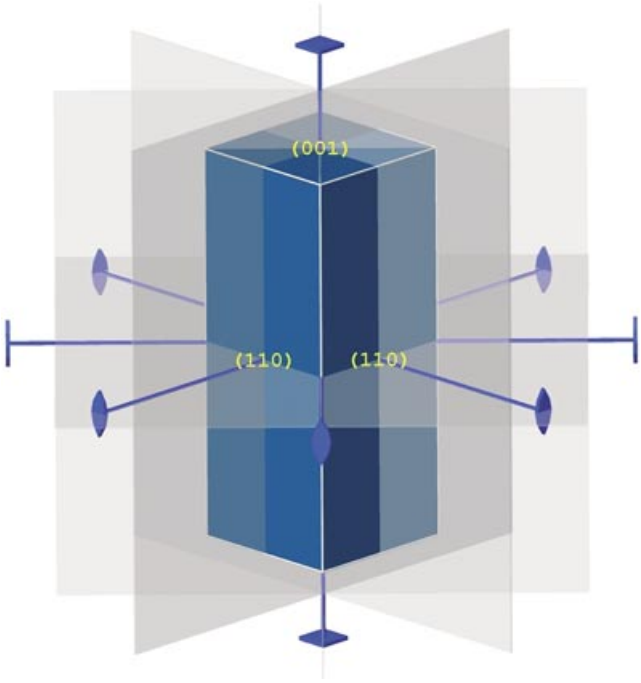

Figure 1. Crystal habit of a rutile SnO_2 (cassiterite) nanorod according to $P4_2/mnm$ symmetry elements and surface energy considerations.

Our strategy to design and control the morphology and orientation of crystallites in large 2D and 3D arrays consists of monitoring the thermodynamics and kinetics of nucleation and growth of metal-oxide materials by controlling experimentally their interfacial tension[16] through a variation of the chemical and electrostatic composition of the water–oxide interface. The synthesis conditions (pH, ionic strength, and

aqueous precursors) are tuned to allow the system to evolve with minimum surface energy, that is, under conditions that are thermodynamically stable. The kinetics are regulated by adjusting the temperature and the concentration of precursors, thus controlling the hydrolysis rate and ratio, which in turn control the nucleation and growth processes. By conducting experiments in solutions that result from the hydrolysis–condensation of aqueous metal-ion precursors (see below), the morphology is therefore dictated by the crystal symmetry as well as by the surface energy in the aqueous environment and thus the most stable crystal habit is generated directly onto the substrates, without template, surfactant, applied field, or undercoating from molecular scale to nano-, meso- or microscale. This concept of "purpose-built nanomaterials",[17] and the thin-film aqueous-growth method[18] have been successfully applied to the fabrication of oriented arrays of basic transition-metal oxides and oxyhydroxides. For instance, the design of large arrays of 3D crystalline highly ordered α-Fe_2O_3,[19] β-FeOOH,[19a] γ-MnOOH,[19b] α-Fe[19c] nanorod arrays, as well as ZnO nanorod,[19d] microrod,[19e] and microtube[19f] arrays have been conducted successfully to illustrate the capability of such an approach.

In accordance with the above-mentioned growth concept, the synthesis was conducted by hydrolysis–condensation of hydrated metal cations by aqueous thermohydrolysis of Sn^{IV} centers in acidic medium with reagent-grade chemicals. Urea, $(NH_2)_2CO$ (also called carbamide or carbonyl diamine) is a nonionic, nontoxic, inexpensive, stable, crystalline, and water-soluble compound. It was chosen to afford simultaneously hydrolysis–condensation by olation of the tetravalent Sn^{IV} ion, most probably from the of zero-charge complex $[Sn(OH)_4(H_2O)_2]$, and the nucleation and growth of its stable dioxide form, rutile SnO_2, by oxolation (the formation of oxo bridges by the elimination of water) from the slow release of hydroxyl ions owing to the well-known thermal decomposition of urea in aqueous solutions. A typical synthesis involved the preparation of a 100 mL aqueous solution (MilliQ+, 18.2 MΩcm) consisting of 0.034 g of $SnCl_4{\cdot}5H_2O$ and 0.920 g of $(NH_2)_2CO$ in presence of 5 mL of fuming HCl (37%) in a closed pyrex bottle with autoclavable screw cap. A large, polycrystalline F–SnO_2 glass substrate (e.g., Hartford Glass Inc. TEK-8), silicon or silicon oxide wafer, or a bare piece of glass (e.g., microscope glass slide), cleaned with diluted acid, ethanol, acetone, subsequently rinsed with MilliQ water, and dried in air was placed standing against the walls of the closed bottle. Thereafter, the bottle was placed in a regular laboratory oven and heated at a constant temperature of 95°C for 2 days. Subsequently, the fully covered and homogeneous thin films were thoroughly washed with water (MilliQ) to remove any possible contamination from residual salts. Fully covered and uniform arrays of several tens of centimeters square, and potentially much larger with larger substrate and container, may be easily produced at very low cost and in a reasonable amount of time.

As expected from the thermodynamic and crystal-symmetry arguments, crystalline nanorods with square cross sections and well-defined crystallographic faces are grown directly onto the substrates. These nanorods, which are typically 50 nm in width and about 500 nm in length (aspect ratio 1:10), are generally perpendicular and arranged in very-large uniform arrays (Figure 2). According to electron and X-ray diffractions, cassiterite (SnO_2 with the rutile structure) is

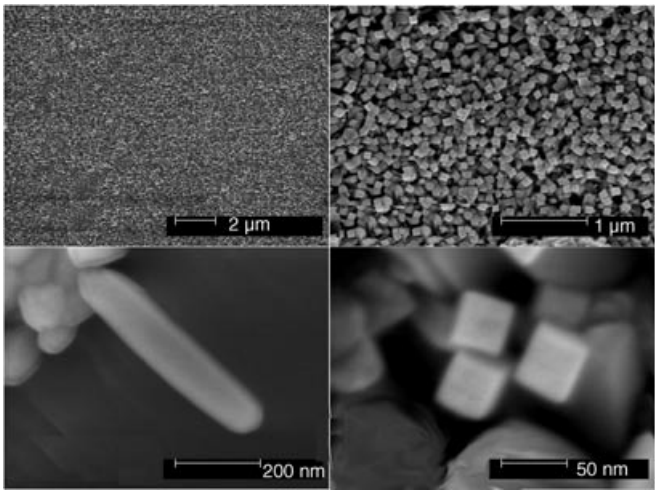

Figure 2. Field-emission gun scanning electron microscopy (FEGSEM) images of SnO_2 nanorods and oriented nanorod arrays, which have a square cross section and have been grown on a TCO glass substrate by controlled aqueous growth.

the only crystallographic phase detected, without significant shift of the lattice spacing compared to bulk SnO_2 (Figure 3). Refinements yield lattice parameters equal to 4.754 and 3.175 Å for *a* and *c*, respectively. The thin film XRD pattern, whose intensity has been normalized to the strongest reflection, shows a substantial texture effect in accordance with the crystal shape anisotropy and orientation. The relative maximum intensity sequence is no longer $(110) > (101) > (211) > (200) > (301) \approx (310) \approx (220) \gg (002) \gg (111) \gg (210)$ but $(101) > (110) > (211) \gg (002) \approx (200) \approx (112) > (301) \approx (111) \approx (220) > (310)$.

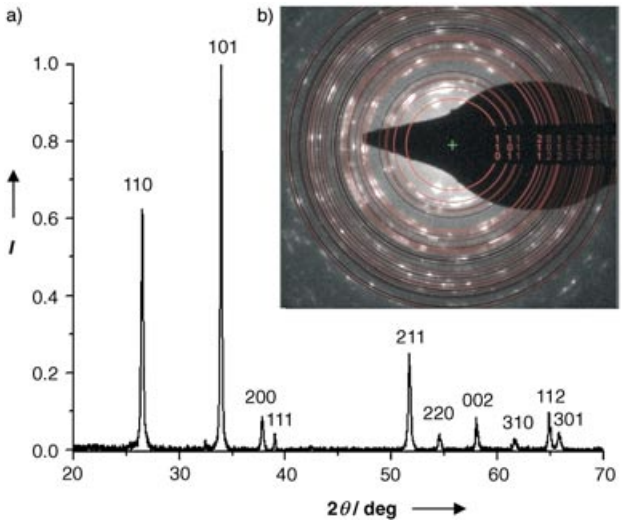

Figure 3. a) Indexed electron and b) X-ray diffraction patterns of SnO_2 nanorods and oriented nanorod-arrays, respectively. *I* is intensity.

As-prepared nanorods are polycrystalline as illustrated by high-resolution (HR) TEM observations (Figure 4) and consist of bundles of finer nanorods of about 2–4 nm in width (aspect ratio of about 1:100). The spacing of the lattice

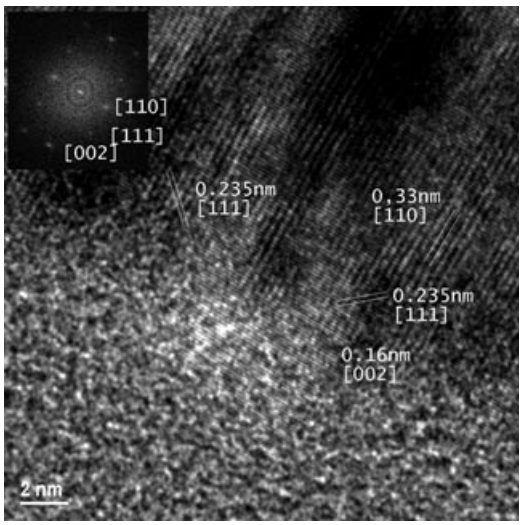

Figure 4. HRTEM and Fourier transform images of a typical SnO_2 nanorod bundle consisting of finer nanorods.

fringes was found to be 0.33, 0.235, and 0.16 nm and these planes are best indexed as (110), (111), and (002) of rutile SnO_2, respectively. Accordingly, the direction of growth of the SnO_2 nanorods is along the *c* axis and with side and top faces consisting of (110) and (001) planes, respectively.

Besides the great stability of (110) faces, it was demonstrated that this surface provides the best efficiency for the chemisorption and dissociation of oxygenated compounds at the SnO_2 interface owing to the lowest interatomic distances between tin atoms (compared to (101) and (111) faces).[20] This factor in particular is of crucial importance for the improvement of the efficiency of SnO_2 photocatalytic and sensing devices. Given that the exposed prismatic faces of the SnO_2 nanorods presented here are the most stable (110) faces, such unique architecture, that is, *c*-elongated and squared cross section with well-defined faces, confers to these arrays a great potential for the development of innovative and functional SnO_2 nanosensors. For instance, better sensitivity and selectivity is foreseen due to the optimized exposed faces as well as a fast response (lower latency time) due to the direct growth of the nanorod bundles onto various substrates, their perpendicular orientation and their anisotropy along the *c* axis, which offers a direct and very efficient electron pathway. Finally, such arrays are excellent candidates for a better fundamental understanding of the electronic-structure and quantum-confinement effects of anisotropic nanocrystals, for example, by polarization-dependent soft-X-ray spectroscopic studies[21] as well as for modeling and simulation studies of interfacial interactions and structure–reactivity relationships of 1D metal oxide nanostructures.

Received: February 11, 2004
Revised: April 22, 2004 [Z54000]

Keywords: nanostructures · nanotechnology · thin films · tin · water chemistry

[1] L. Vayssieres in *Encyclopedia of Nanoscience and Nanotechnology, Vol. 8* (Ed.: H. S. Nalwa), American Scientific Publishers, Stevenson Ranch, CA, **2004**, pp. 147–166; a) Z. R. Dai, Z. W. Pan, Z. L. Wang, *Adv. Funct. Mater.* **2003**, *13*, 9–24.
[2] T. Minami, *MRS Bull.* **2000**, *25(8)*, 38–44; E. Elangovan, K. Ramamurthi, *J. Optoelectron. Adv. Mater.* **2003**, *5*, 45–54.
[3] Y. Shimizu, T. Hyodo, M. Egashira, *J. Eur. Ceram. Soc.* **2004**, *24*, 1389–1398; C. O. M. Su, S. Li, V. P. Dravid, *J. Am. Chem. Soc.* **2003**, *125*, 9930–9931M. Law, H. Kind, B. Messer, F. Kim, P. D. Yang, *Angew. Chem.* **2002**, *114*, 2511; *Angew. Chem. Int. Ed.* **2002**, *41*, 2405; P. G. Harrison, M. J. Willet, *Nature* **1988**, *332*, 337–339.
[4] N. Park, M. G. Kang, K. S. Ryu, K. M. Kim, S. H. Chang, *J. Photochem. Photobiol. A* **2004**, *161*, 105–110; G. Benko, P. Myllyperkio, J. Pan, A. P. Yartsev, V. Sundstrom, *J. Am. Chem. Soc.* **2003**, *125*, 1118–1119; T. Hasobe, H. Imahori, P. V. Kamat, S. Fukuzumi, *J. Am. Chem. Soc.* **2003**, *125*, 14962–14963; C. Bauer, G. Boschloo, E. Mukhtar, A. Hagfeldt, *Int. J. Photoenergy* **2002**, *4*, 17–20; M. Graetzel, *Nature* **2001**, *414*, 338–344; a) P. R. Bueno, E. R. Leite, T. R. Giraldi, L. O. S. Bulhoes, E. Longo, *J. Phys. Chem. B* **2003**, *107*, 8878–8883; N. Li, C. R. Martin, B. Scrosati, *Electrochem. Solid-State Lett.* **2000**, *3*, 316–318.
[5] D.-F. Zhang, L.-D. Sun, J.-L Yin, C.-H. Yan, *Adv. Mater.* **2003**, *15*, 1022–1025; a) Y. Liu, C. Zheng, W. Wang, C. Yin, G. Wang, *Adv. Mater.* **2001**, *13*, 1883–1887.
[6] Y. Liu, C. Zheng, W. Wang, Y. Zhan, G. Wang, *J. Cryst. Growth* **2001**, *233*, 8–12.
[7] C. Xu, G. Xu, Y. Liu, X. Zhao, G. Wang, *Scr. Mater.* **2002**, *46*, 789–794.
[8] Y. Wang, X. Jiang, Y. Xia, *J. Am. Chem. Soc.* **2003**, *125*, 16176–16177.
[9] Y. Chen, X. Cui, K. Zhang, D. Pan, S. Zhang, B. Wang, J. G. Hou, *Chem. Phys. Lett.* **2003**, *369*, 16–20.
[10] Z. Liu, D. Zhang, S. Han, C. Li, T. Tang, W. Jin, X. Liu, B. Lei, C. Zhou, *Adv. Mater.* **2003**, *15*, 1754–1757.
[11] W. Wang, C. Xu, X. Wang, Y. Liu, Y. Zhan, C. Zheng, F. Song, G. Wang, *J. Mater. Chem.* **2002**, *12*, 1922–1925.
[12] A. Kolmakov, Y. Zhang, M. Moskovits, *Nano Lett.* **2003**, *3*, 1125–1129; J. K. Jian, X. L. Chen, T. Xu, Y. P. Xu, L. Dai, M. He, *Appl. Phys. A* **2002**, *75*, 695–697.
[13] A. Kolmakov, Y. Zhang, G. Sheng, M. Moskovits, *Adv. Mater.* **2003**, *15*, 997–1000; M. Zheng, G. Li, X. Zhang, S. Huang, Y. Lei, L. Zhang, *Chem. Mater.* **2001**, *13*, 3859–3861.
[14] M. Batzill, K. Katsiev, U. Diebold, *Surf. Sci.* **2003**, *529*, 295; V. A. Gercher, D. F. Cox, J.-M. Themlin, *Surf. Sci.* **1994**, *306*, 279–293; D. F. Cox, T. B. Fryberger, S. Semancik, *Phys. Rev. B* **1988**, *38*, 2072–2083; a) A. Beltran, J. Andres, E. Longo, E. R. Leite, *Appl. Phys. Lett.* **2003**, *83*, 635–637; J. Oviedo, M. J. Gillan, *Surf. Sci.* **2000**, *463*, 93–101; P. A. Mulheran, J. H. Harding, *Modell. Simul. Mater. Sci. Eng.* **1992**, *1*, 39–43.
[15] L. B. Fraigi, D. G. Lamas, N. E. W. de Reca, *Mater. Lett.* **2001**, *47*, 262; C. Xu, X. Zhao, S. Liu, G. Wang, *Solid State Commun.* **2003**, *125*, 301–304; a) J. X. Wang, D. F. Liu, X. Q. Yan, H. J. Yuan, L. J. Ci, Z. P. Zhou, Y. Gao, L. Song, L. F. Liu, W. Y. Zhou, *Solid State Commun.* **2004**, *130*, 89–94.
[16] L. Vayssieres, *Int. J. Nanotechnol.* **2004**, *1*, 1–41; L. Vayssieres, *J. Colloid Interface Sci.* **1998**, *205*, 205–212; L. Vayssieres, PhD thesis, Université Pierre et Marie Curie (Paris), **1995**.
[17] L. Vayssieres, A. Hagfeldt, S.-E. Lindquist, *Pure Appl. Chem.* **2000**, *72*, 47–52.
[18] L. Vayssieres, *Int. J. Mater. Prod. Technol.* **2003**, *18*, 313–337; L. Vayssieres, A. Hagfeldt, S.-E. Lindquist, Patent WO9935312, **1999**, pp. 1–49.

[19] L. Vayssieres, N. Beermann, S.-E. Lindquist, A. Hagfeldt, *Chem. Mater.* **2001**, *13*, 233 – 235; a) L. Vayssieres, J.-H. Guo, J. Nordgren, *Mater. Res. Soc. Symp. Proc.* **2001**, *635*, 781 – 786; b) L. Vayssieres, A. Manthiram, *Mater. Res. Soc. Symp. Proc.* **2003**, *739*, 249 – 254; c) L. Vayssieres, L. Rabenberg, A. Manthiram, *Nano Lett.* **2002**, *2*, 1393 – 1395; d) L. Vayssieres, *Adv. Mater.* **2003**, *15*, 464 – 466; e) L. Vayssieres, K. Keis, S.-E. Lindquist, A. Hagfeldt, *J. Phys. Chem. B* **2001**, *105*, 3350 – 3352; f) L. Vayssieres, K. Keis, A. Hagfeldt, S.-E. Lindquist, *Chem. Mater.* **2001**, *13*, 4395 – 4398.

[20] V. Brinzari, G. Korotcenkov, V Golovanov, J. Schwank, V. Lantto, S. Saukko, *Thin Solid Films* **2002**, *408*, 51 – 58; D. Kohl, *Sens. Actuators* **1989**, *18*, 71; M. Egashira, T. Matsumoto, Y. Shimizu, H. Iwanaga, *Sens. Actuators* **1988**, *14*, 205; V. Brinzari, G. Korotcenkov, S. Dmitriev, *Sens. Actuators B* **1999**, *61*, 143 – 153.

[21] J.-H. Guo, L. Vayssieres, C. Persson, R. Ahuja, B. Johansson, J. Nordgren, *J. Phys. Condens. Matter* **2002**, *14*, 6969 – 6974.

